Optical design of split-beam photonic crystal nanocavities

Aaron C. Hryciw[1,*] **and Paul E. Barclay**[(1,2)]

[1] *National Institute for Nanotechnology, 11421 Saskatchewan Drive, Edmonton, Alberta, Canada, T6G 2M9*
[2] *Institute for Quantum Information Science, University of Calgary, 2500 University Drive NW, Calgary, Alberta, Canada, T2N 1N4*
[*] *Corresponding author: Aaron.Hryciw@nrc-cnrc.gc.ca*

Compiled January 7, 2013

Photonic crystal nanobeam cavities are attractive due to their high quality factors, small mode volume, low effective mass, and small physical footprint. Here we demonstrate that a high quality factor photonic crystal nanobeam can be formed by two mechanically isolated cantilevers. The resulting cavity has a physical gap in the center, enabling independent mechanical motion of one or both of the cavity halves. By considering the optical band structure and mode profiles of silicon waveguides perforated by elliptical holes and rectangular gaps, such "split-beam cavity" designs with quality factors exceeding 10^6 at free-space resonance wavelengths of $\sim$1.6 μm are achieved in finite-difference time-domain electromagnetic simulations.

Photonic crystal (PC) nanobeam cavities [1] are currently the subject of intense research interest, possessing a suite of attractive characteristics—high optical quality factor (Q), wavelength-scale effective mode volume (V_{eff}), low effective mass, and small physical footprint. Integrated within planar photonic waveguide circuitry, PC nanobeam cavities provide a chip-based architecture for applications including single particle sensing [2], quantum information processing [3], nonlinear optics [4], optofluidics [5], and cavity optomechanics [6–8]. Many sensing applications are poised to benefit from orders of magnitude improvements in measurement sensitivity enabled by on-chip cavity optomechanics, for example, measurement of nanostring mechanical resonators [9], inertial sensing [10], novel platforms for chip-based AFM [11], and detection of torsional motion for magnetometery applications [12,13]. To maximize the sensitivity of these measurements, it is desirable to use devices whose central cavity region is not rigid [14], and can be easily deformed by external forces [6,11,15]. To this end, we describe in this Letter the optical design of a PC nanobeam cavity in which the cavity region adiabatically transforms to a structure with a complete cut through the nanobeam . This yields a device geometry in which two mechanically uncoupled nano-cantilevers form an optical cavity with high Q that may support a wide range of mechanical excitations.

The archetypal PC nanobeam cavity is based on the quasi-1D PC waveguide: a dielectric beam perforated by a periodic array of holes. To form an optical cavity from this structure, a geometric feature—e.g., hole size/shape/spacing, waveguide width—is tapered symmetrically about the cavity center. This dielectric perturbation yields a spatially-varying optical potential which supports localized modes within the optical band-gap of the host waveguide [16]. As the principal Fourier components of these bound modes are confined near the edges of the first Brillouin zone, the cavity mode profiles and frequencies can largely be understood by examining the band-edge behavior of the underlying periodic waveguides. Indeed, it is possible to design PC nanobeam cavities with ultra-high Q ($>10^9$) deterministically, through band-edge frequency considerations only, circumventing the need to optimize Q via computationally-expensive trial-and-error-based parameter searches [17]. Here we consider embedding a complete gap in the center of a conventional PC nanobeam cavity formed in a waveguide patterned with air holes, and find that by careful consideration of the anomalous ordering of the band-

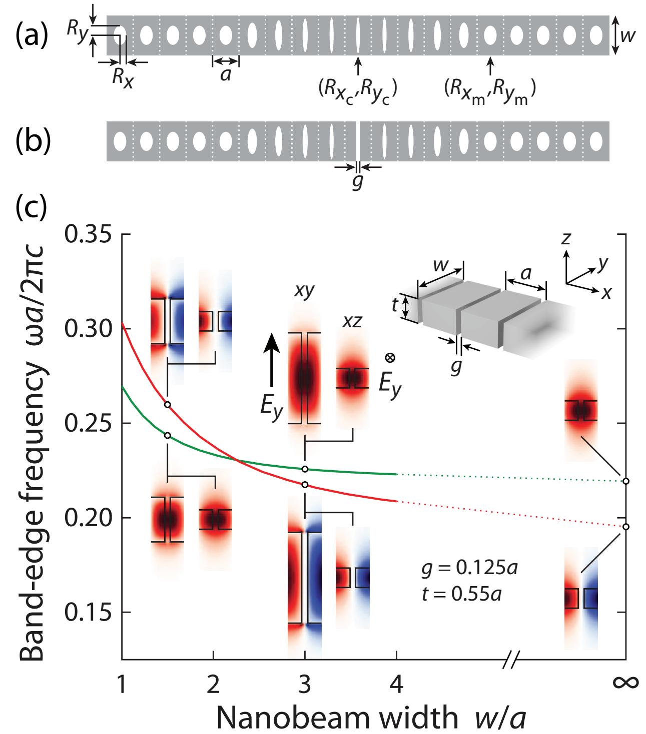

Fig. 1. (a) Schematic of donor-mode nanobeam cavity with elliptical holes. (b) Schematic of "split-beam" cavity with a rectangular gap defect at center. (c) "Gap unit cell" band-edge frequencies and electric field profiles for TE-like (y-odd, z-even) modes as a function of nanobeam width. For the mode profiles, the dominant E_y component is plotted for the xy and xz planes.

edge mode of the gap unit cell, a high-Q cavity can be realized.

We begin with the deterministic design approach of Quan *et al.* [17, 18], summarized as follows. Choose a central unit cell geometry (waveguide cross-section, hole size and shape) such that the band-edge frequency of a waveguide mode supported by a periodic array of this cell with lattice constant a approximately matches the desired resonance frequency $\omega_{\rm res}$. The overall spatial symmetry of the cavity mode is determined by the symmetry of this waveguide mode. For example, a cavity with $\omega_{\rm res}$ aligned with the central unit cell valence (conduction) band will have its field concentrated in the dielectric (air), and is referred to as an acceptor (donor) mode. The acceptor (donor) modes are said to have odd (even) x symmetry upon reflection about a yz plane through the hole center. Next, to minimize power leakage into the waveguide, choose a "mirror" unit cell geometry which maximizes the mirror strength γ with respect to $\omega_{\rm res}$; this is equivalent to choosing a geometry for which $\omega_{\rm res}$ is mid gap and the band-gap is maximized. Near the band-edge, the wavevector may be approximated by $k_x = (1+i\gamma)\frac{\pi}{a}$, with

$$\gamma = \left[\left(\frac{\omega_2-\omega_1}{\omega_2+\omega_1}\right)^2 - \left(\frac{\omega_{\rm res}-\omega_0}{\omega_0}\right)^2\right]^{\frac{1}{2}} \qquad (1)$$

where ω_1 and ω_2 are the lower and upper (respectively) band-edge frequencies defining the optical band-gap of a periodic waveguide, and ω_0 is the mid-gap frequency [18]. To minimize out-of-plane scattering into radiation modes—the dominant loss process limiting the overall cavity Q—the geometry is smoothly tapered over several segments, such that γ varies linearly between the central ($\gamma = 0$) and mirror ($\gamma = \gamma_{\rm max}$) unit cells. Finally, two such half-cavities are placed back-to-back and capped on either end with several more mirror segments to complete the cavity design; a generalized donor-mode cavity with elliptical holes is shown in Figure 1a, tapering from the central hole $(R_{x_{\rm c}}, R_{y_{\rm c}})$ to the mirror hole $(R_{x_{\rm m}}, R_{y_{\rm m}})$ over six segments.

A plausible (albeit naïve) program to construct an optomechanical sensor based on a PC nanobeam cavity would be to start with a high-Q design as explained above and simply cut the nanobeam at the cavity center, yielding a "split-beam" cavity capable of supporting a wide variety of mechanical modes (e.g., axial, torsional, in- and out-of-plane). The mechanical oscillation frequency, quality factor, and effective mass could then be tuned by an appropriate choice of nanobeam supports [15]. Choosing a donor-mode cavity, where the field is concentrated in the air regions, allows the field maximum to be placed in the central gap; this field can then interact strongly with modulation of the gap width from mechanical excitations. Without careful design, however, such a gap can can compromise the adiabaticity of the cavity taper, causing severe scattering into radiation modes and reducing Q by several orders of magnitude. To minimize such scattering, intuition suggests that the central hole unit cell be replaced with a gap unit cell whose relevant band-edge frequency and spatial field profile closely match those of the hole.

To evaluate this proposed design quantitatively, we begin by analyzing a PC waveguide comprising a periodic array of dielectric blocks with lattice constant a (along $\hat{x}$) and thickness t, separated by gaps of width g. Figure 1c shows the band-edge frequencies and field profiles (E_y) for the first two TE-like (y-odd, z-even) modes as the block width w varies, calculated using a 3D frequency-domain eigensolver [19] with a spatial discretization of 32 per period a. A constant relative permittivity of $\epsilon = 12.11$ is used throughout, corresponding to that of silicon at a free-space wavelength of 1550 nm, and the gaps are centered at $x = 0$.

Understanding the crossing of the band-edge frequencies as w/a decreases, shown in Fig. 1c, is crucial to successfully designing an nanobeam cavity incorporating a central gap. In the 2D limit the crossing may be explained by considering the mode profiles and properties of 1D and 2D photonic crystals [20]: the field of the fundamental TE mode (red line) is concentrated in the dielectric (E_y odd in x), yielding a higher effective index (lower band-edge frequency) than in the second TE mode (green line), in which the field maximum is in the low-ϵ air gap (E_y even in x). As w/a decreases, however, the stronger dispersion of the "dielectric" mode relative to the "air" mode causes these modes to cross in frequency (at $w/a \approx 2.25$ for this geometry); for values of w/a smaller than this crossing point, the lower-energy TE-like mode is therefore an "air" mode. This difference in dispersion can be understood from the perturbation theory developed by Johnson *et al.* [21] which accurately accounts for the vectorial nature and associated discontinuous boundary conditions of Maxwell's equations in wavelength-scale nanophotonic structures. When w/a is decreased, the "dielectric" mode frequency experiences a larger shift because it overlaps more strongly with the moving waveguide boundary than the "air" mode, whose field is concentrated in the central air region which undergoes no change in shape. Note that this crossing behavior is not exhibited in photonic crystal nanobeam waveguides with a hole in place of the gap for the considered range of w/a.

This cross-over is therefore of crucial importance to split-beam cavity design based on the methodology of [17], for it governs which of the two gap unit cell modes should be used to determine the cavity resonance frequency and overall symmetry: the central hole must be replaced with a rectangular gap for which the band-edge frequency of the *air mode* (whether this is the the first or second TE-like mode, depending on the nanobeam cross-section) matches that of the central hole.

To illustrate this design paradigm, we investigate three cavities with air-mode resonance wavelengths around 1.6 μm, suitable for fabrication using silicon-on-insulator (SOI) wafers. For a Si ($\epsilon = 12.11$) nanobeam with thickness $t = 220$ nm, width $w = 600$ nm, and periodicity $a = 400$ nm, a gap of width $g = 50$ nm corresponds to Figure 1c with $w/a = 1.5$: the "air" mode is the lowest-energy TE-like mode. In Figure 2, we compare the band structure of this rectangular gap with that of three elliptical holes satisfying the matching condition: the "air"-mode band-edge frequencies of the holes and the gap are equal ($\omega_{\mathrm{res}}a/2\pi c$=0.2435). For y semi-axes of 275, 175, and 75 nm, this is satisfied using x semi-axes of 28.8, 33.6, and 52.6 nm, respectively. The field profiles of the band-edge modes for the elliptical holes are shown adjacent to their associated bands, where we observe the intuitive behavior in which the lowest-energy TE-like mode is of the acceptor ("dielectric") type.

With two parameters defining their shape—the x and y semi-axes—elliptical holes afford the possibility of satisfying the matching condition with a continuum of hole shapes, plotted with the yellow line in Figure 3. The mirror strength γ is calculated for a range of ellipse shapes using (1); as shown in Figure 3, the maximum occurs at $(R_{x_{\mathrm{m}}}, R_{y_{\mathrm{m}}}) = (100, 140)$ nm. To maintain a small nanobeam cavity footprint, we taper the ellipses between the central $(R_{x_{\mathrm{c}}}, R_{y_{\mathrm{c}}})$ and mirror $(R_{x_{\mathrm{m}}}, R_{y_{\mathrm{m}}})$ shapes over $N_{\mathrm{c}} = 7$ holes, capping each half-cavity with $N_{\mathrm{m}} = 8$ more holes of shape $(R_{x_{\mathrm{m}}}, R_{y_{\mathrm{m}}})$. We achieve an approximately linear variation of γ between the central and mirror holes by tapering both semi-axes quadratically: $R_{x_j,y_j} = R_{x_{\mathrm{c}},y_{\mathrm{c}}} + (j/N_{\mathrm{c}})^2(R_{x_{\mathrm{m}},y_{\mathrm{m}}} - R_{x_{\mathrm{c}},y_{\mathrm{c}}})$, for integer $j \in [-N_{\mathrm{c}}, N_{\mathrm{c}}]$. The half-cavity ($j \in [0, N_{\mathrm{c}}]$) hole shapes for the three cavities defined by the central elliptical holes considered in Figure 2 are plotted as open circles in Figure 3. The central ($j = 0$) ellipse is then replaced by a 50-nm-wide rectangular gap to complete the design. Note that, up to this point, only band-structure calculations have been used in the design, as in [17].

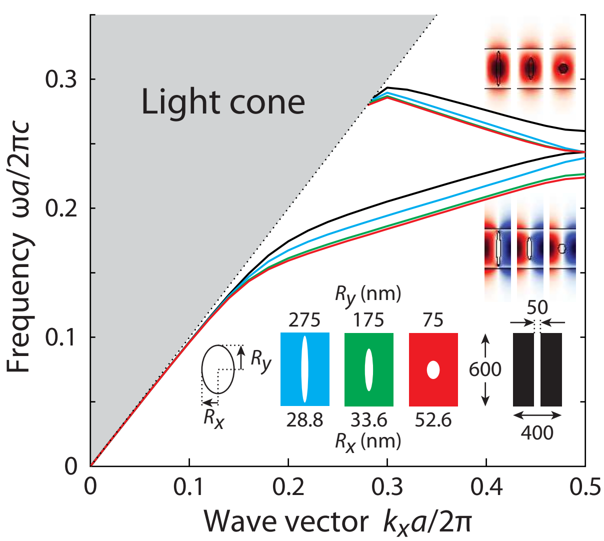

Fig. 2. Band structures for an infinite periodic array of rectangular gaps and three elliptical holes exhibiting the split-beam cavity matching condition at the band edge. The geometries of the unit cells are shown in the inset (all units in nm); the nanobeam thickness is 220 nm. Field profiles of the dielectric (lower) and air (upper) modes for the elliptical holes are shown next to their associated bands.

We assess the performance of these three cavities using finite-difference time-domain (FDTD) simulations [22]; the field profiles for each are shown in Figure 3b, with Q, λ_{res}, and V_{eff} listed in the inset to Figure 3a. The overall cavity Q is dominated by scattering perpendicular to the nanobeam, split nearly evenly in the y and z directions; loss into guided modes (x direction) is small due to the large γ of the mirror segments. While all three cavities satisfy the band-edge matching condition described above, significantly less scattering occurs as the fictitious "central ellipse" more closely resembles the cross-section of a rectangular gap (i.e., large R_y), achieving a Q of $3.3{\times}10^6$ for the $R_{y_{\mathrm{c}}}$=275 nm cavity. As elucidated in [23], coupling from from the band-edge waveguide modes into lossy radiation modes generally increases as a taper between waveguide cross-sections becomes less gradual. In the case of the $R_{y_{\mathrm{c}}}$=75 nm cavity, the poor adiabaticity between the gap and the neighboring hole degrades the Q to 3.6×10^4.

While the Q could in principle be increased for this choice of N_{c} and N_{m} by further optimizing the cavity holes, we note that the band-edge matching condition yields $(R_{x_{\mathrm{c}}}, R_{y_{\mathrm{c}}})$ values which are very close to optimal for a quadratic taper: a free maximization of Q with respect to $R_{x_{\mathrm{c}}}$ using FDTD yields only a $\sim$20% improvement in Q for the $R_{y_{\mathrm{c}}}$=275 and 175 nm cavities, with a change in $R_{x_{\mathrm{c}}}$ of less than 10%. Alternately, Q may be increased—at the expense of a larger V_{eff} and cavity footprint—by increasing N_{c} to yield a more adiabatic taper [17].

From an experimental standpoint, Figure 3a illustrates the inherent trade-off in this scheme between Q and practical fabricability: pattern fidelity becomes more difficult for long, narrow elliptical holes due to minimum feature size limits in electron-beam lithography and dry etching processes.

By considering the photonic band structure of a nanobeam cut through by a periodic array of rectangular air gaps, we have demonstrated how a deterministic design algorithm for PC nanobeam cavities can be modified to yield "split-beam" cavities which exhibit a high optical quality factor ($>10^6$) despite the existence of a major perturbation in the cavity region. The resulting cavity supports a mode whose electromagnetic energy density is concentrated in the central air gap, and is well-suited to sensing applications involving actuation of the mechanically uncoupled sections of the nanocavity. This will be particularly useful for applications such as optomechanical force sensing and torque magnetometry [13].

We thank M. H. Wu, J. D. Davis, and M. R. Freeman for helpful discussions. This work was supported by NRC, CFI, AITF, and NSERC.

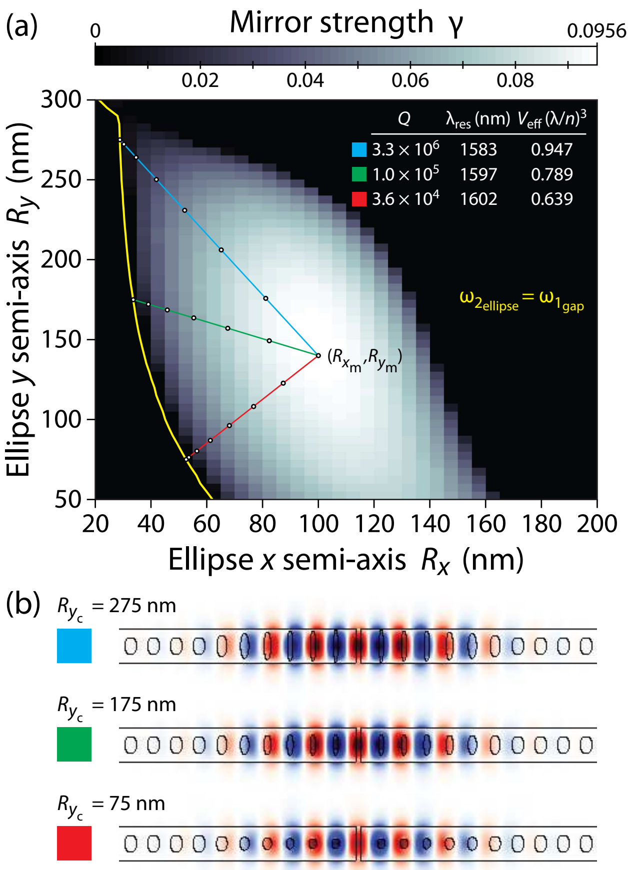

Fig. 3. (a) Mirror strength and resulting design parameters for three split-beam cavities; a, t, and w, and the three (R_{x_c}, R_{y_c}) values are as in Figure 2. The half-cavity tapered ellipse shapes are shown by open circles. (b) Mode profiles (E_y, xy plane) of the three cavities in (a).

References

1. M. Notomi, E. Kuramochi, and H. Taniyama, "Ultrahigh-Q Nanocavity with 1D Photonic Gap," Opt. Express **16**, 11 095 (2008).
2. I. Mukherjee, G. Hajisalem, and R. Gordon, "One-step integration of metal nanoparticle in photonic crystal nanobeam cavity," Opt. Express **19**, 22 462–22 469 (2011).
3. M. W. McCutcheon and M. Lončar, "Design of an ultrahigh Quality factor silicon nitride photonic crystal nanocavity for coupling to diamond nanocrystals," Opt. Express **16**, 19 136 (2008).
4. P. E. Barclay, K. Srinivasan, and O. Painter, "Nonlinear response of silicon photonic crystal microresonators excited via an integrated waveguide and a fiber taper," Opt. Express **13**, 801–820 (2005).
5. S. Mandal and D. Erickson, "Nanoscale optofluidic sensor arrays," Opt. Express **16**, 1623–1631 (2008).
6. M. Eichenfield, R. Camacho, J. Chan, K. J. Vahala, and O. Painter, "A picogram- and nanometre-scale photonic-crystal optomechanical cavity." Nature **459**, 550–5 (2009).
7. M. Eichenfield, J. Chan, R. M. Camacho, K. J. Vahala, and O. Painter, "Optomechanical crystals," Nature **462**, 78–82 (2009).
8. P. B. Deotare, I. Bulu, I. W. Frank, Q. Quan, Y. Zhang, R. Ilic, and M. Loncar, "All optical reconfiguration of optomechanical filters." Nat. Comm. **3**, 846 (2012). http://www.ncbi.nlm.nih.gov/pubmed/22617286
9. E. Gavartin, P. Verlot, and T. Kippenberg, "A hybrid on-chip optomechanical transducer for ultrasensitive force measurements," Nat. Nano **7**, 509514 (2012).
10. A. G. Krause, M. Winger, T. D. Blasius, Q. Lin, and O. Painter, "A high-resolution microchip optomechanical accelerometer," Nature Phot. **6**, 768–772 (2012).
11. K. Srinivasan, H. Miao, M. T. Rakher, M. Davanço, and V. Aksyuk, "Optomechanical transduction of an integrated silicon cantilever probe using a microdisk resonator," Nano letters **11**, 791 (2011).
12. J. P. Davis, D. Vick, D. C. Fortin, J. A. J. Burgess, W. K. Hiebert, and M. R. Freeman, "Nanotorsional resonator torque magnetometry," Appl. Phys. Lett. **96**, 72 513 (2010).
13. P. H. Kim, C. Doolin, B. D. Hauer, A. J. R. MacDonald, M. Freeman, P. E. Barclay, and J. P. Davis, "Nanoscale Torsional Optomechanics," arXiv preprint arXiv:1210.1852 (2012).
14. M. Li, W. Pernice, and H. Tang, "Broadband all-photonic transduction of nanocantilevers," Nature Nano. **4**, 377–382 (2009).
15. M. H. Wu, A. C. Hryciw, and P. E. Barclay, "Torsional optomechanics," (2012), (In preparation).
16. O. Painter, K. Srinivasan, and P. E. Barclay, "Wannier-like equation for the resonant cavity modes of locally perturbed photonic crystals," Phys. Rev. B **68**, 35 214 (2003).
17. Q. Quan and M. Lončar, "Deterministic design of wavelength scale, ultra-high Q photonic crystal nanobeam cavities," Opt. Express **19**, 18 529–18 542 (2011).
18. Q. Quan, P. Deotare, and M. Lončar, "Photonic crystal nanobeam cavity strongly coupled to the feeding waveguide," Appl. Phys. Lett. **96**, 203 102–203 102 (2010).
19. S. G. Johnson and J. D. Joannopoulos, "Block-iterative frequency-domain methods for Maxwell's equations in a planewave basis," Opt. Express **8**, 173–190 (2001). http://www.opticsexpress.org/abstract.cfm?URI=OPEX-8-3-173
20. J. Joannopoulos, S. Johnson, J. Winn, and R. Meade, *Photonic Crystals: Molding the Flow of Light* (Princeton University, 2008).
21. S. G. Johnson, M. Ibanescu, M. A. Skorobogatiy, O. Weisberg, J. D. Joannopoulos, and Y. Fink, "Perturbation theory for Maxwell's equations with shifting material boundaries," Phys. Rev. E **65**, 66 611 (2002).
22. A. F. Oskooi, D. Roundy, M. Ibanescu, P. Bermel, J. D. Joannopoulos, and S. G. Johnson, "MEEP: A flexible free-software package for electromagnetic simulations by the FDTD method," Comp. Phys. Comm. **181**, 687–702 (2010). http://www.sciencedirect.com/science/article/B6TJ5-4XRJX96-3/2/97a9289cb9e2b8524b86e1112c1b593b
23. S. G. Johnson, P. Bienstman, M. A. Skorobogatiy, M. Ibanescu, E. Lidorikis, and J. D. Joannopoulos, "The adiabatic theorem and a continuous coupled-mode the-

ory for efficient taper transitions in photonic crystals,"
Phys. Rev. E **66**, 66 608 (2002).